A HYBRID NAVAL HYDRODYNAMIC SCHEME BASED ON AN EFFICIENT LATTICE BOLTZMANN METHOD COUPLED TO A POTENTIAL FLOW SOLVER

Christopher O'Reilly[1,2], Stephan Grilli[1], Jason Dahl[1], Christian F. Janssen[3], Amir Banari[3], J.J. Shock[1], Micha Uberrueck[3]

[1]University of Rhode Island, Department of Ocean Engineering, Narragansett, Rhode Island, USA
[2]Navatek LTD, South Kingstown, Rhode Island, USA
[3]Fluid Dynamics and Ship Theory Inst., Hamburg University of Technology, Germany

This paper details the development of a 3D coupled approach between a boundary element method potential flow model, for the large- to near-field scale, and a Navier-Stokes model in the near-field, based on a velocity and pressure decomposition approach. We focus on the development of a new viscous solver, intended for this coupling, which is based on the Lattice Boltzmann Method. The solver uses a large eddy simulation of the turbulence and volume of fluid free surface capturing method. The method is validated by simulating an advancing surface piercing hydrofoil for which there are both published and new laboratory experiments; hence, this case represents a rigorous benchmark for the proposed free surface solver.

KEY WORDS
Lattice Boltzmann; Finite Difference Lattice Boltzmann; Hybrid Viscous Methods

INTRODUCTION
The simulation of large ship motions and resistance in steep waves is typically performed using linear or nonlinear potential flow solvers usually based on higher-order Boundary Element Methods (BEM), with semi-empirical corrections introduced to account for viscous/turbulent effects. However in some cases viscous effects near the ship's hull and breaking waves and wakes need to be accurately modeled to capture the relevant physics. Navier-Stokes (NS) solvers can and have been used to model these problems, but they are computationally expensive and often too numerically dissipative to model wave propagation over long distances.

Here, we detail the development of a 3D coupled approach, based on a perturbation approach (i.e., a velocity and pressure decomposition; Harris and Grilli, 2012), between a BEM nonlinear potential flow model, referred to as Numerical Wave Tank (NWT), simulating the large- to near-field scales, and a NS model simulating the near-field. Developments of the NWT, which is optimized with a Fast Multipole Method (FMM), and its more recent optimization on large parallel clusters have been reported elsewhere (e.g., Grilli et al., 2010; Harris et al., 2014). In this paper, we focus on the development and validation of an efficient free-surface NS solver, to be used in this coupling method, based on the Lattice Boltzmann Method (LBM; e.g., d'Humieres et al., 2002; Janssen, 2010; Janssen et al., 2010). In the LBM, turbulence is modeled by a Large Eddy Simulation (LES; Krafczyk et al., 2003) and the free surface is captured using the volume of fluid (VOF) method. While the NWT based on a FMM-BEM is optimized to achieve nearly linear scaling on large CPU clusters (Harris et al., 2014), the LBM is implemented on a massively parallel General Purpose Graphical Processor Unit (GPGPU) co-processor; other work has shown that LBM models can achieve a very high efficiency on such hardware (over 100 million node updates per second on a single GPGPU; e.g., Janssen, 2010; Janssen et al., 2013; Banari et al., 2014).

We first describe the two-way unsteady perturbation coupling approach being used to solve fluid body interaction problems (Janssen et al., 2010). Next, we detail the development of the LBM model and present results of a simple validation application of the coupling approach for a viscous oscillatory Boundary Layer (BL; Janssen, 2010). We then further validate the LBM based on experimental results alongside a comparison with results of the potential flow model Aegir.

The LBM has proved to be accurate and efficient for simulating a variety of complex fluid flow and fluid-structure interaction problems (e.g., Banari et al., 2014; Janssen et al., 2010, 2013). Hence, in the context of the field decomposition approach, the combination of a LBM only applied to the near-field, with a fast BEM potential flow solver applied to the entire domain, in a hybrid approach, LBM has the potential for a much increased computational efficiency relative to traditional CFD approaches in which a NS solver is applied over the entire domain. This was already demonstrated, based on other less optimized models, by Reliquet et al. (2014). One reason for high efficiency of the LBM is the inherent locality of its collision-propagation operators, allowing for linear scalability for parallel computing on GPGPU units. Furthermore, recent developments in LBM modeling allow for the accurate and stable simulation of high Reynolds number flows (e.g., Banari et al., 2014).

Once the relevance of the coupling approach is demonstrated for an oscillatory wave BL, the LBM scheme is validated through an advancing surface piercing hydrofoil test case, representing a rigorous benchmark for the free surface solver. Such a foil has all the characteristics and is thus a simpler proxy for a ship with a more complex hullform. A large set of new well-controlled

laboratory experiments for an advancing vertical, surface-piercing, foil with NACA 0012 profile was performed at the University of Rhode Island, to serve as a rigorous validation of the various numerical models, as well as their coupling approach. Here, the measured free surface geometry and velocity field around the foil are compared with model simulations for a range of Froude numbers.

DECOMPOSITION COUPLING APPROACH

Let us first illustrate the decomposition-coupling approach in a simple case of viscous flow and consider the NS equations for an incompressible, isothermal, Newtonian fluid:

$$\frac{\partial u_i}{\partial x_i} = 0 \quad (1)$$

$$\frac{\partial u_i}{\partial t} + \frac{\partial}{\partial x_j}\left(u_i u_j + \frac{p}{\rho}\delta_{ij} - \nu\frac{\partial u_i}{\partial x_j}\right) = 0 \quad (2)$$

Where u_i and p are the water velocity and dynamic pressure, respectively, in a fluid of density ρ and kinematic viscosity ν. We introduce a decomposition of the flow into the sum of an inviscid component and defect or perturbation flow component.

$$u_i = u_i^I + u_i^P \quad (3)$$

$$p = p_I + p_P \quad (4)$$

When only considering the inviscid flow fields, Eqs. (1) and (2) yield Euler's equations:

$$\frac{\partial u_i^I}{\partial x_i} = 0 \quad (5)$$

$$\frac{\partial u_i^I}{\partial t} + \frac{\partial}{\partial x_j}\left(u_i^I u_j^I + \frac{p_I}{\rho}\delta_{ij}\right) = 0 \quad (6)$$

Inserting Eqs. (3) and (4) into Eqs. (1) and (2), and applying Eqs. (5) and (6), the remaining terms represent the governing equations for the perturbation field

$$\frac{\partial u_i^P}{\partial x_i} = 0 \quad (7)$$

$$\frac{\partial u_i^P}{\partial t} + \frac{\partial}{\partial x_j}\left(u_i u_j - u_i^I u_j^I + \frac{p_P}{\rho}\delta_{ij} - \nu\frac{\partial u_i}{\partial x_j}\right) = 0 \quad (8)$$

Based on Kelvin's theorem, Eqs. (5) and (6) can be exactly solved with a potential flow solver, when the flow is started from a state of rest, which provides the inviscid flow fields to force Eqs. (7) and (8). The latter equations can be directly solved with a standard NS solver (e.g., as in Harris and Grilli, 2012 and Reliquet et al., 2014). However here, as detailed later, Eqs. (7) and (8) will be solved with a LBM in which the inviscid forcing terms will be treated as volume forces in the collision operator.

In the context of an unsteady ship simulation, viscous forcing terms are typically insignificant far from the body, where the flow can accurately be modeled in a potential flow solver. As the body is approached, turbulent, and then viscous effects, as well as breaking waves around the bow and stern, influence the flow, which requires solving the full NS equations. In the decomposition coupling approach, however, only the perturbation flow fields need to be solved for in the neighborhood of the ship, which for highly streamlined bodies will typically yield a much smaller computational domain than when applying a CFD NS code to the entire problem.

More specifically, we set up our computational domains so that the potential flow model is used throughout the entire domain and satisfies boundary conditions on the ship's hull, whether considering a steady advancing ship in still water or a more complex seakeeping problem for an advancing ship in a complex sea state. A small NS solver domain, linked to the ship, extends out from the hull until viscous effects become small enough to be neglected. The potential flow model serves to drive the NS solver through both boundary conditions and the forcing terms present in Eq. 8. The total solution may then be reconstructed based on the combined solution from each solver. Note that the nonlinear free surface dynamic and kinematic boundary conditions must be expressed for the total flow fields, in order to update the free surface geometry and kinematics to the next time level. This requires reconciling the different representations of the free surface made in the potential flow NWT and in the NS model, at each time step, and must be carefully and accurately done (see, e.g., Reliquet et al., 2014). Additional numerical problems must be tackled, particularly at the free surface intersection with the surface piercing bodies. Further development of this will be detailed in future work.

THE LATTICE BOLTZMANN METHOD

The LB method has become an increasingly efficient and widely used approach for solving a variety of difficult fluid dynamics problems. In contrast with classical CFD solvers, which are dealing with the macroscopic NS equations on a continuum basis, the LBM solves CFD problems on a mesoscopic scale and represents the fluid as a field of interacting particle distribution functions $f(t,\mathbf{x},\boldsymbol{\xi})$ on a lattice (i.e., regular mesh). Macroscopic hydrodynamic quantities can be obtained from low order moments of these distribution functions (see, e.g., d'Humieres et al., 2002). The efficiency and accuracy of the LBM method have been demonstrated in many publications. One key feature if the method is that it can be efficiently parallelized to benefit from massively parallel hardware. Recently, GPGPU implementations of a LB method have achieved remarkable performances of over 100 million lattice nodes updates per second on a single graphics processing units; large GPGPU clusters (of typically a few hundred GPGPUs) have achieved teraflop performances.

The primary variable in the original "microscopic" Boltzmann equation is the particle distribution function $f(t,\mathbf{x},\boldsymbol{\xi})$, which specifies the normalized probability to encounter a particle at position $\mathbf{x}$ at time t with velocity $\boldsymbol{\xi}$. The evolution of such distribution functions f is described by the Boltzmann equation:

$$\frac{\partial f(\mathbf{x},t,\mathbf{v})}{\partial t} + \mathbf{v}\cdot\frac{\partial f(\mathbf{x},t,\mathbf{v})}{\partial \mathbf{x}} = \Omega \quad (9)$$

The left-hand side of this equation is an advection-type expression, while the collision operator Ω describes the interactions of particles on the microscopic scale. In order to obtain a model with reduced computational cost, the Boltzmann equation is discretized over a lattice in the velocity space $\boldsymbol{\xi}$. In this work, the D3Q19 model is used (Fig. 1), which introduces

the following 19 discretized mesoscopic particle velocities $\boldsymbol{e_i}$={0,0,0},{±c,0,0},{0,±c,0},{0,0,±c},{±c,±c,0},{±c,0,±c}, {0,±c,±c}, i = 0, . . . ,18, where the constant velocity c is related to the speed of sound c_s=c/√3. The resulting set of discrete Boltzmann equations,

$$\frac{\partial f_i(\mathbf{x},t)}{\partial t} + e_i \cdot \frac{\partial f_i(\mathbf{x},t)}{\partial \mathbf{x}} = \Omega_i \qquad (10)$$

have to be discretized in space and time. This is done using a standard first-order finite difference scheme, in space and time, on a lattice of grid spacing Δx, with $c = \Delta x/\Delta t$, with time step Δt. This yields the lattice Boltzmann equation:

$$f_i(t + \Delta t, \boldsymbol{x} + e_i\Delta t) - f_i(t, \boldsymbol{x}) = \Delta t(\Omega_i + F_i) \qquad (11)$$

where F_i represents effects of volume forces (e.g., here gravitational, viscous, and inviscid forcing). Finally, Eq. (11) is split up into a nonlinear collision step, which drives the particle distribution functions to equilibrium locally, and a nonlocal linear propagation step, where the post-collision particle distribution functions are advected to the neighbor nodes in directions i as (Fig. 1),

$$f_i(t, \boldsymbol{x}) = f_i(t, \boldsymbol{x}) + \Delta t(\Omega_i + F_i) \quad \text{and}$$
$$f_i(t + \Delta t, \boldsymbol{x} + e_i\Delta t) = f_i(t, \boldsymbol{x}) \qquad (12)$$

It has been well-established that solutions of the lattice Boltzmann equation satisfy the incompressible NS equations up to errors of $O(\Delta x^2)$ and $O(\mathrm{Ma}^2)$ (with Ma the Mach number).

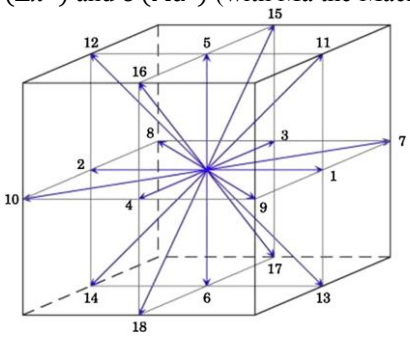

Figure 1: A D3Q19 lattice scheme

The standard macroscopic values for the hydrodynamic pressure and macroscopic fluid velocity are found from the first two hydrodynamic moments of the particle distribution functions as,

$$p(\boldsymbol{x}, t) = c_s^2\rho(\boldsymbol{x}, t) = c_s^2 \sum_{i=0}^{18} f_i(\boldsymbol{x}, t) \qquad (13)$$
$$\boldsymbol{u}(\boldsymbol{x}, t) = \frac{1}{\rho}\sum_{i=0}^{18} \boldsymbol{e}_i f_i(\boldsymbol{x}, t) \qquad (14)$$

where ρ denotes the fluid density. For modelling the interactions between particles, different collision operators Ω_i have been proposed, in the context of viscous fluid flows. Here we use the multiple relaxation time (MRT) method (d'Humieres et al., 2002), which has been proven to be stable and accurate for high Reynolds number flows.

Furthermore, consistent with Eq. (8), we use the LBM perturbation coupling method first introduced in Janssen (2010), in which additional terms are added to the MRT collision operator to represent effects of inviscid forcing terms, which are treated as volume forces (formally introduced in Eqs. (11) and (12) as F_i).

LBM IMPLEMENTATION

We use the 3-D LBM solver elbe (developed by Dr. Janssen, Institute for Fluid Dynamics and Ship Theory at Hamburg University of Technology), which is based on a on equidistant Cartesian grids. A nested mesh of increasing resolution may be used in areas of high flow gradients and/or where more accuracy is desired. The Smagorinsky Large Eddy Simulation (LES) model is used to represent turbulence at the sub-grid scale. This is implemented in the LBM model through using a turbulent (eddy) viscosity,

$$\nu_T = (Cs\Delta v)^2||\boldsymbol{S}|| \qquad (15)$$

Where Cs represents the Sagorinsky constant and $\boldsymbol{S}$ represents a local strain rate tensor. The details of this implementation within the LBM context can be found in Krafczyk et al. (2003) and Janssen et al. (2010).

In the following, we detail two methods used for free surface representation, the Volume of Fluid (VOF) free surface interface capturing method, which the is the standard method used in elbe to model free surface flows, and the Level set interface tracking method, which provides for a smoother functional representation of the interface and has been shown to perform better in the present context (e.g., Reliquet et al., 2014). In the future, the LS method will be implemented in elbe.

Volume of Fluid Interface Capturing

In the Volume of Fluid (VOF) free surface interface capturing method a cell's fill level, ϵ is followed in time,

$$\epsilon = \frac{V_{fluid}}{V_{cell}} \qquad (16)$$

A fill level of 0.0 marks an empty cell in the inactive gas domain above the free surface, and a fill level of 1.0 corresponds to a filled cell inside the fluid domain. Fluid and gas cells are separated by a closed interface layer (Figure 2) with a fill level between 0.0 and 1.0. In the LB context, we assign a VOF control volume to one lattice node. In order to calculate the evolution of the free surface in time, an additional advection equation has to be solved. The mass flux between two cells is evaluated in terms of particle distribution functions f_i as,

$$\Delta m_i = [f_I(\boldsymbol{x}, t) - f_i(\boldsymbol{x}, t)] \cdot A_i \qquad (17)$$

where I is the opposite direction to I, and A_i represents the wet area between two cells, which is estimated as the arithmetic mean of the fill level of two neighboring cells:

$$A_i = \begin{cases} 1.0 & : neighbor\ fluid\ cell \\ \frac{\epsilon(x,t)+\epsilon(x+e_i,t)}{2} & : neighbor\ interface\ cell \\ 0.0 & : neighbor\ gas\ cell \end{cases} \quad (18)$$

In contrast with higher-order schemes, the normal vector information is not considered here. Hence, this first-order approach in space does not conserve all line (2D) or plane (3D) segments exactly between two time steps. Once the flux terms have been evaluated, the new fill level of a cell can be calculated as,

$$\epsilon^{n+1} = \frac{\rho^n \epsilon^n + \sum_i \Delta m_i}{\rho^{n+1}} \quad (19)$$

Where $\rho^{n,n+1}$ is the fluid density at time step n or n+1, respectively, and the same convention applies to ϵ. After fill levels have been updated, several rules must be applied for initializing new nodes and correcting ϵ. These are detailed in Jansen (2010).

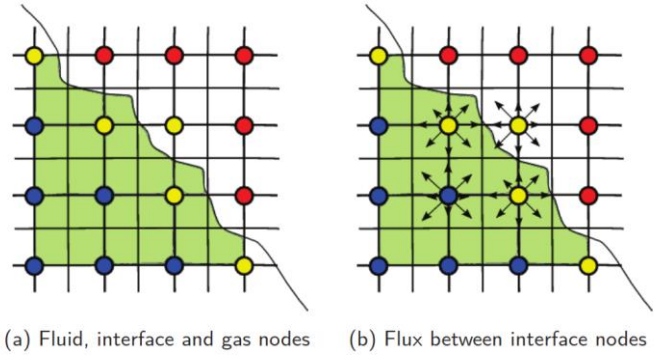

Figure 2: Fluid (blue), interface (yellow), and gas (red) nodes in the VOF method

Level Set Interface Tracking

In this interface tracking approach, a smooth level set (LS) function, ϕ is introduced, which represents the signed distance of a cell center to the free surface interface. The free surface is then reconstructed as the zero-distance isosurface of the signed distance field. However, for the interface advection, no surface reconstruction is needed, but the motion of the surface is simply described by the advection of the LS function as,

$$\frac{\partial \phi}{\partial t} + u_i \frac{\partial \phi}{x_i} = 0 \quad (20)$$

Since the LS function is smooth and continuous across the interface, its gradient can be accurately calculated.

The LS approach is beneficial in the present hybrid method context due to the inherent decomposition of the boundary conditions at the free surface. Just as done above in the NS equations, the pressure and velocity decomposition must also be applied to the kinematic and dynamic free surface boundary conditions, which leads to interactions between the potential flow and LBM solvers. Therefore, neither the potential flow nor the LBM solution will represent the correct free surface geometry and kinematics, and one must reconstruct the correct free surface at each time step, based on the complete solution with the complete boundary conditions. Furthermore if the complete free surface is above the potential flow free surface an extrapolation will be necessary to compute the inviscid forcing fields needed in Eq. (8). The smooth and accurate free surface representation provided by the LS method will be important in this context. Figure 3 illustrates the representation of the same interface with the VOF fill or LS functions.

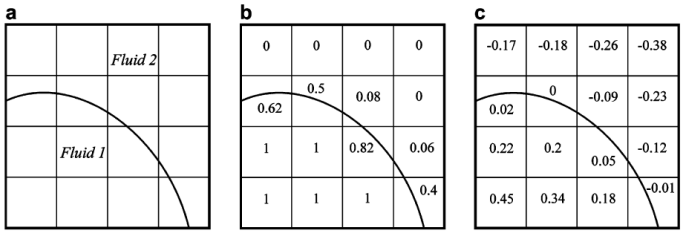

Figure 3: A comparison of the VOF (b) and LS (c) free surface representation of a free surface interface (a).

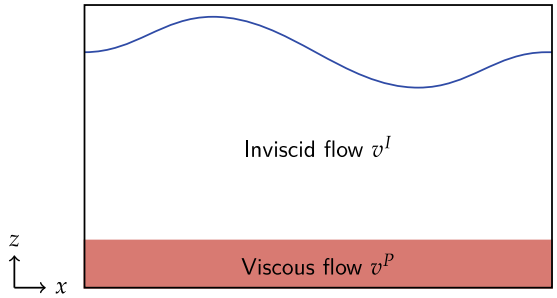

Figure 4: Set up for two-dimensional (2D) Oscillatory Viscous Wave Boundary Layer (OVWBL) problem.

HYBRID COUPLING PROOF OF CONCEPT

Janssen (2010) and Janssen et al. (2010) first proposed to solve the perturbation Eqs. (7) and (8) based on a LBM. To do so, the inviscid forcing terms were represented as volume forces, similarly to gravity or viscous/turbulent forces, in the LBM, which we formally denote as F_i in Eqs. (11) and (12). The relevance of this representation was verified by solving the simple 2D problem of an Oscillatory Viscous Wave Boundary Layer (OVWBL; Fig. 4). Longuet-Higgins (1953) first showed that, even when considering the linear wave theory (LWT) potential to force a viscous boundary layer (BL) near a solid wall, a steady current is generated (referred to as "steady streaming") for which he developed the following analytical solution,

$$u = \frac{A^2 \omega k}{\sinh^2 kh}\left[\frac{3}{4} - e^{-\xi}\cos\xi + \frac{1}{2}e^{-\xi}\sin\xi + \frac{1}{4}e^{-2\xi} - \frac{1}{2}\xi e^{-\xi}\cos\xi - \frac{1}{2}\xi e^{-\xi}\sin\xi\right] \quad (21)$$

where u denotes the wall parallel velocity as a function of the non-dimensional distance to the wall $\zeta = z/\delta_s$ (where δ_s denotes the theoretical viscous BL thickness for a kinematic viscosity ν), for a wave of amplitude A, angular frequency ω, wavenumber k, in depth h.

A proof of concept of the hybrid coupling field decomposition approach is provided here by solving the 2D-OVWBL problem with the modified LBM code solving Eqs. (7) and (8), with the inviscid velocity fields u_i^I given by the LWT potential. For the simulation, we use: A = 0.01 m, ω = 10.47 r/s, k = 12.57 m^{-1}, h = 0.113 m. The LBM domain is $2\pi/k$ = 0.5 m long in the x direction and $16\delta_s$ = 0.05 m high in the vertical z direction (where δ_s is computed with ν = 5.11 10^{-5} m^2/s). The solution was computed until steady state was reached, in four regular LBM grids with 100 x 10, 200 x 20, 400 x 40 and 800 x 80 cells in the x and z directions, respectively.

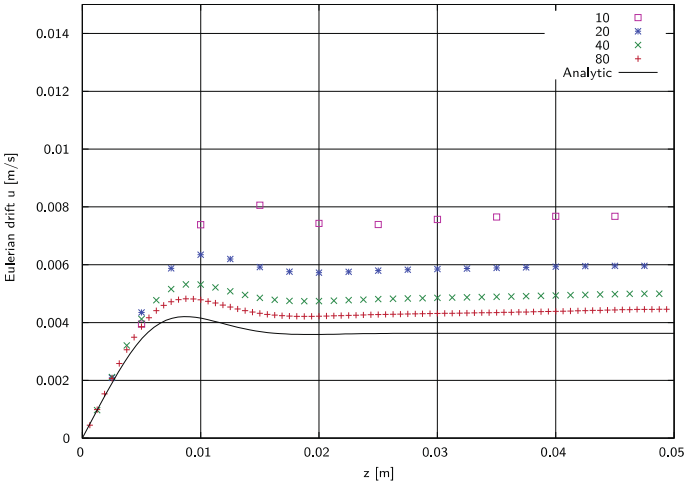

Figure 5: Comparison of LBM and analytical results for the steady streaming velocity *u* in a (2D) Oscillatory Viscous Wave Boundary Layer as a function of distance *z* to the wall.

In the LBM solution, in addition to a periodicity condition in the x direction we use the following boundary conditions in the z direction,

$$\mathbf{v}^P(z=0) = -\mathbf{v}^I(z=0) \quad \text{and} \quad \partial_z \mathbf{v}^P(y=16\delta_s) = \mathbf{0} \tag{22}$$

where the first condition ensures a no-slip condition on the rigid wall and the second one specifies a vanishing gradient of the viscous perturbation away from the wall.

Figure 5 compares the LBM solution in the four tested grids (obtained assuming a low Mach value Ma = 0.001) to the analytical solution from Eq. (21). We see both a clear convergence of the numerical solution to the reference solution with, in the finer grid, a good agreement between both. This hence, confirms the relevance of the proposed hybrid coupling of a potential and LBM solver in a perturbation scheme.

ADVANCING FOIL VALIDATION TEST SETUP

As the hybrid method under development involves overlapping solutions of two numerical methods, there is particular concern related to proper estimation of the free surface, both in each model and for the complete solution. It is also desirable to obtain an experimental data set for validating the numerical scheme, once all parts are implemented and operational in a general context; this includes forces, 3-D velocity field, and free surface elevation for a surface piercing body. Previous experimental data sets contain good measurements of free surface characteristics and surface pressures on the body, yet few studies contain volumetric measurements of velocity or pressure that could be used for validation in the overlapping numerical domains of the potential and LBM models.

To address the limitations of previous experiments, a new set of laboratory experiments have been conducted, yielding quantitative flow visualization of the velocity field and free surface elevations generated by a surface piercing foil. The foil is used here as a relevant proxy for a more complex hullform. In these experiments, a NACA 0012 foil, with chord length 70 mm and submerged span of 275 mm, is towed with constant velocity in a precision tow tank, to achieve Froude numbers based on chord length of Fn = 0.19, 0.37, and 0.55.

Elbe simulations of these tests were conducted, using the parameters detailed in Table 1. A time step of 0. 47 ms was used in the coarsest level. The simulations were run on a single NVIDIA Tesla K20 GPGPU (with 2496 cores and 5 Gb RAM) and required less than 1h to achieve several seconds of steady state conditions for each test.

Grid Level	Δx[m]	Size [m]			Nodes			Total/Nodes
		x	y	z	x	y	z	
1	0.0025	0.45	0.32	0.32	180	128	128	2,949,120
2	0.00125	0.3	0.17	0.14	240	136	112	3,626,800
3	0.000625	0.21	0.154	0.1	336	246	160	13,224,960
								19,802,880

Table 1: Elbe mesh parameters for advancing foil case

Concurrently the high-order BEM solver Aegir was run, in its linear and steady formulation. A discretization independent test setup was found and velocity information outputted in the region of interest. Computational time for 1 Aegir simulation required roughly 5 minutes using 1 CPU. An additional fully nonlinear NWT that is being developed as part of this project; was also run. Results of this model, however, will not be detailed here but be left out for future papers.

RESULTS

A comparison of the velocity field near the foil calculated by elbe and Aegir with the measured data is provided in the appendix. Plots show the normalized downstream component of the velocity measured at horizontal slices at different depths. The measured data presented represents an average velocity over many repeated experiments, while the average velocity estimated in elbe was evaluated over the steady state portion of the simulation. Overall, a general agreement in the velocity magnitudes and flow structure may be seen. A clear wake region may be seen in elbe, where viscous effects are dominant. Within the wake region, a large variance of the velocity field relative to the overall field is observed, as vortex shedding occurs. A region

of less accurate experimental data may be observed in the shallowest slice (Fn=0.37), which is likely the result of insufficient particle seeding within the region, during measurements. A larger interrogation window within this region is likely necessary to properly evaluate velocities within the region. As velocity increases, the free surface's influence becomes more prevalent within the velocity field, resulting from the formation of wakes of larger amplitude and wavelength.

A comparison of the free surface estimated by elbe and Aegir may be seen in Figure 6. An over-prediction of the free surface elevation occurs in Aegir results, at the middle and highest Froude numbers, largely due to increasing nonlinearity in the free surface wave field, as well as viscous/turbulent dissipations that result (particularly where breaking occurs), which are not captured in the linearized potential flow solution provided by Aegir; a breaking bow wave is likely occurring at these speeds. Moreover, linear waves are not properly estimating the diffracted component of the solution. At the lower Froude number, insufficient free surface discretization is seen in elbe and free surface waves are not simulated due to their short wavelength. For this case, the linear solver is likely reasonably estimating the wave field as very little numerical dissipation is observed. The small variation of the velocity field with depth (Figure A1) observed within the Aegir simulation likely shows that these waves are not largely important in influencing the pressure distribution on the foil.

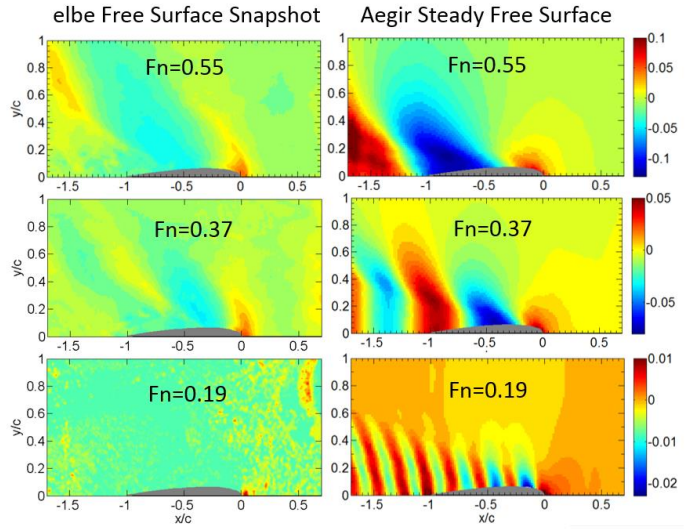

Figure 6: Free surface comparison of elbe (left) and Aegir (right) at varying speeds (rows). Results shown for elbe represent the free surface at 1 time step.

Currently, only one free surface elevation measurement is available along a free surface slice. Figure 7 shows the measured average free surface and a band representing three standard deviations of it. The measured bow wave presented here is likely incorrect due to high free surface curvature and location of the camera. A recent interpretation of these results (not shown here) shows that this bow wave is higher with a much reduced variance. Elbe and Aegir results are also shown. Several free surface slices from different time steps in elbe were evaluated and results generally fall within the free surface measurement envelope. A region where elbe is poorly predicting the free surface is seen between *x/c*=0.4 through *x/c*=0.55. This is the location of the seperation point predicted by elbe and flow re-circulation is present. This overprediction of viscous effects is likely the result of underdiscritization.

CONCLUSIONS

These results represent a start towards the hybrid method implementation, which show both a validation of the hybrid coupling approach between potential flow and LBM solvers for a simple OVWBL case near a solid wall, as well as a general match between elbe results and measurements for an advancing foil. Further validation must be conducted, including a full free surface comparison and the evaluation of the pressures acting on the foil. Additionally, results of the fully nonlinear NWT must be included in the comparison. These validations may be done when further processing of measured results are completed.

A validation of the LS method will be conducted using the same test cases, leading to an initial hybrid method implementation, which may be conducted using a steady state potential flow solution. A focus will be directed towards implementing the proper fee surface boundary representation.

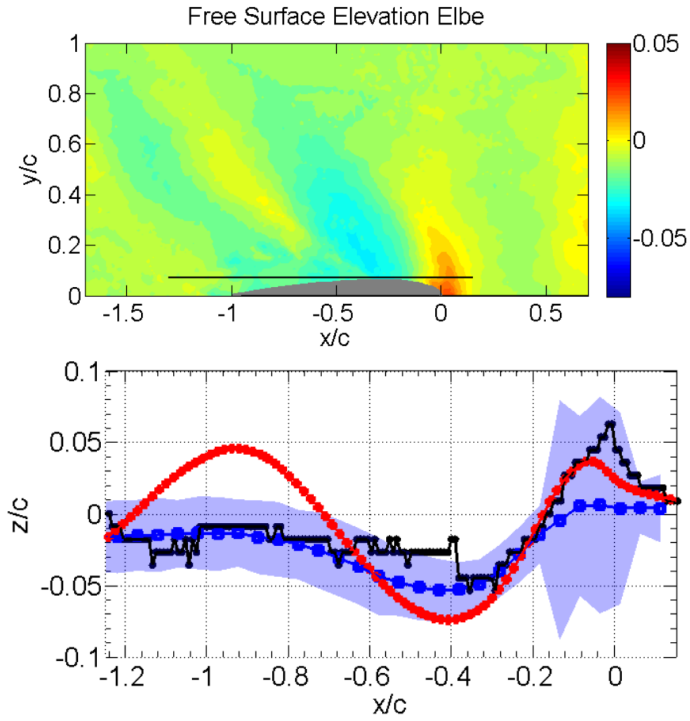

.Figure 7: Free surface elevations measured at the line showed in black in the top image. The measured average free surface and three standard deviations of it are shown as the blue line and blue shaded area, respectively. The Aegir prediction is in red while the elbe prediction is in black.

ACKNOWLEDGEMENTS

This work was supported by the Office of Naval Research, PM Kelly Cooper. The authors gratefully acknowledge this support.

REFERENCES

Banari A., Janssen C.F., and Grilli S.T. 2014. An efficient lattice Boltzmann multiphase model for 3D flows with large density ratios at high Reynolds numbers. *Comp. Math. with Appl.*, **68**, 1819-1843, doi:10.1016/j.camwa.2014.10.009 .

Grilli, S.T., Dias, F., Guyenne, P., Fochesato, C. and F. Enet 2010. Progress In Fully Nonlinear Potential Flow Modeling Of 3D Extreme Ocean Waves. Chapter 3 in *Advances in Numerical Simulation of Nonlinear Water Waves* (ISBN: 978-981-283-649-6, edited by Q.W. Ma) (Vol. 11 in Series in Advances in Coastal and Ocean Engineering). World Scientific Publishing Co. Pte. Ltd., pps. 75- 128.

Harris, J.C. and S.T. Grilli 2012. A perturbation approach to large-eddy simulation of wave-induced bottom boundary layer flows. *Intl. J. Numer. Meth. Fluids*, **68**, 1,574-1,604, doi:10.1002/fld.2553

Harris, J.C., Dombre, E., Benoit, M. and S.T. Grilli 2014. Fast integral equation methods for fully nonlinear water wave modeling. In *Proc. 24th Offshore and Polar Engng. Conf.* (ISOPE14, Busan, South Korea, June 2014), Intl. Society of Offshore and Polar Engng., pps. 583-590.

d'Humieres D., T. Ginzburg, M. Krafczyk, P. Lallemand, and L.-S. Luo 2002. Multiple Relaxation-Time Lattice Boltzmann models in three-dimensions. *Royal Soc. Lond. Phil. Trans.*, **A360**, 437–451.

Janssen C.F., S.T. Grilli and M. Krafczyk 2010. Modeling of Wave Breaking and Wave-Structure Interactions by Coupling of Fully Nonlinear Potential Flow and Lattice-Boltzmann Models. In *Proc. 20th Offshore and Polar Engng. Conf.* (ISOPE10, Beijing, China, June 20-25, 2010), pps. 686-693. Intl. Society of Offshore and Polar Engng.

Janssen, C.F. 2010. *Kinetic approaches for the simulation of non-linear free surface flow problems in civil and environmental engineering*. PhD thesis, Technical University Braunschweig.

Janssen, C.F., S.T. Grilli and M. Krafczyk 2013. On enhanced non-linear free surface flow simulations with a hybrid LBM-VOF approach. *Computers and Mathematics with Applications*, **65**(2), 211-229, doi:10.1016/j.camwa.2012.05.012 (published online 7/12/12).

Krafczyk, M., Tölke, J., and Luo, L.-S. 2003. Large eddy simulations with a multiple-relaxation-time LBE model. *Int. J. Mod. Phys. B*, **17**, 33–39.

Longuet-Higgins, M.S. 1953. Mass transport in water waves. *Phil. Trans. Royal Soc. London*, **A**, 535–581.

Reliquet, G., A. Drouet, P.-E. Guillerm, L. Gentaz and P. Ferrant 2014. Simulation of wave-ship interaction in regular and irregular seas under viscous flow theory using the SWENSE method. In *Proc. 30th Symposium on Naval Hydrodynamics* (Hobart, Tasmania, Australia, 2-7 November, 2014), 11 pps.

APPENDIX: VELOCITY COMPARISON

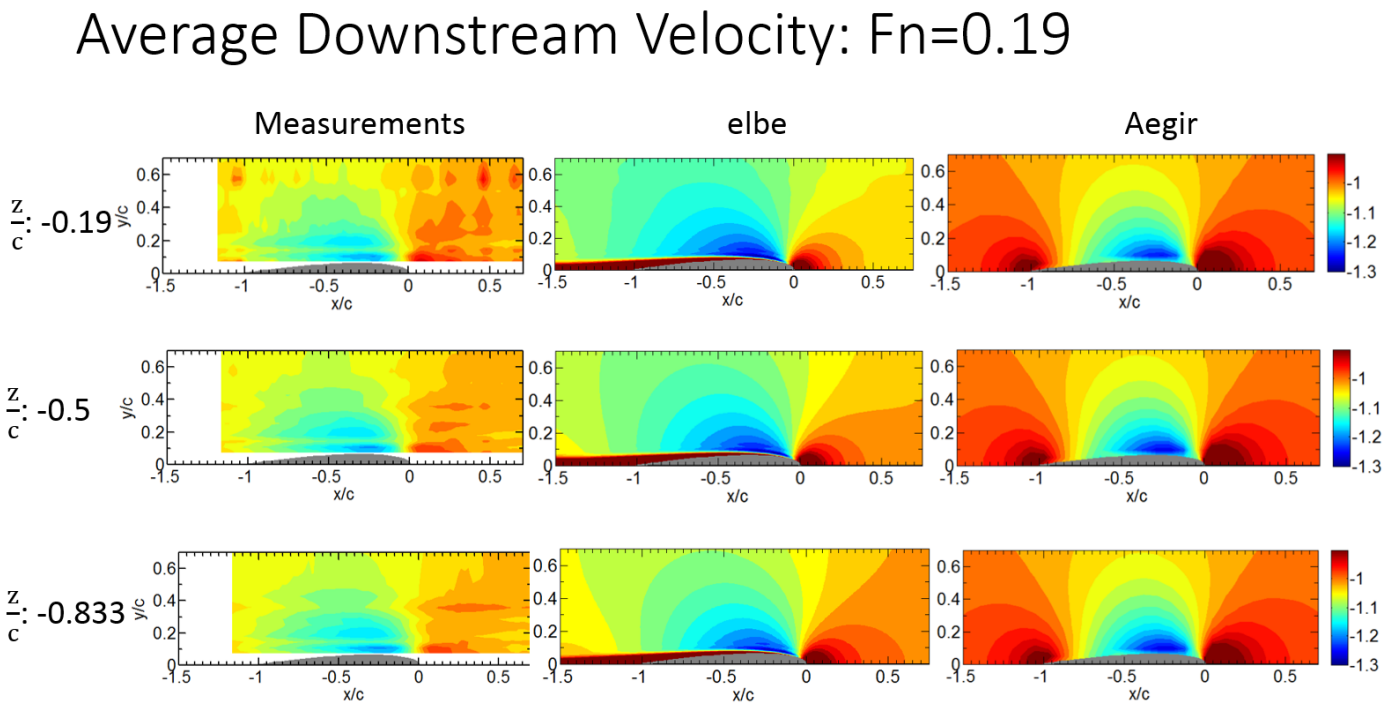

Figure A1: Downstream velocities shown at different depths (rows) at a Froude number of 0.19. Measured data (left) are averaged over all tests while elbe (middle) velocities were averaged over 5 seconds of steady state. Linear steady state velocities from Aegir may be seen on the left.

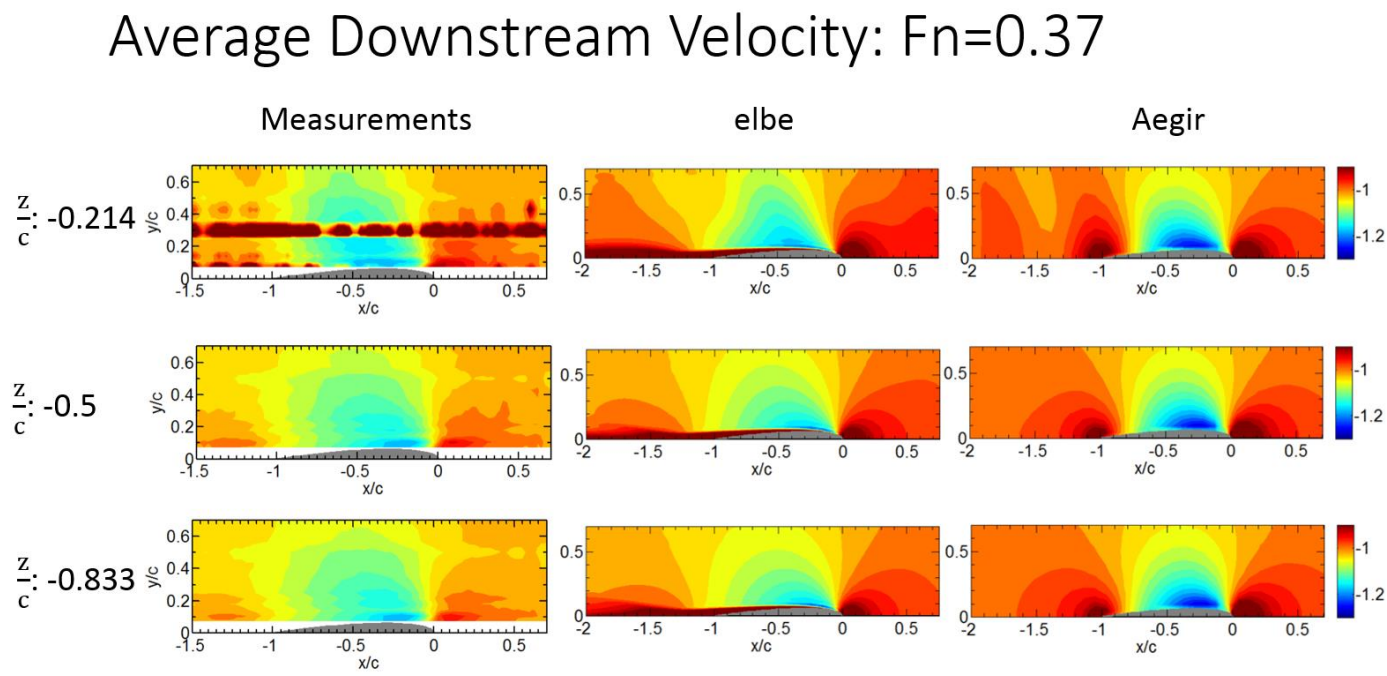

Figure A2: Downstream velocities shown at different depths (rows) at a Froude number of 0.37. Measured data (left) are averaged over all tests while elbe (middle) velocities were averaged over 5 seconds of steady state. Linear steady state velocities from Aegir may be seen on the left.

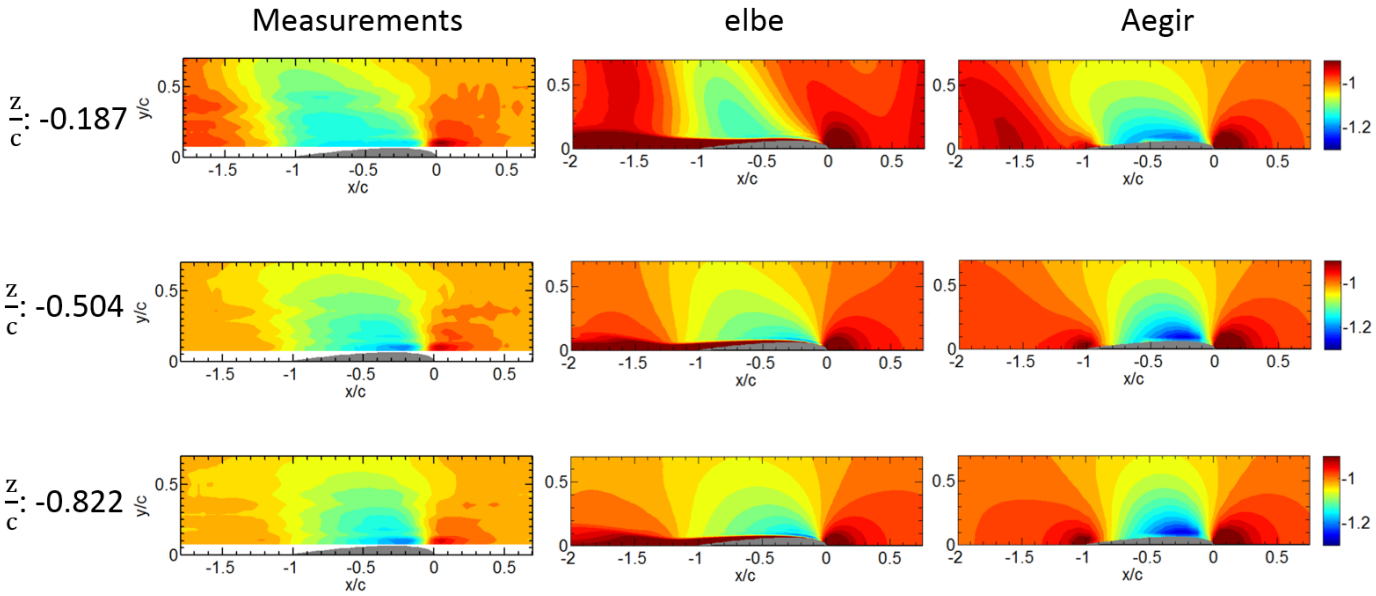

Figure A3: Downstream velocities shown at different depths (rows) at a Froude number of 0.55. Measured data (left) are averaged over all tests while elbe (middle) velocities were averaged over 5 seconds of steady state. Linear steady state velocities from Aegir may be seen on the left.